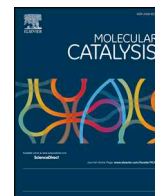




ELSEVIER

Contents lists available at ScienceDirect

Molecular Catalysis

journal homepage: www.elsevier.com/locate/mcat

Immobilization of (tartrate-salen)Mn(III) polymer complexes into SBA-15 for catalytic asymmetric epoxidation of alkenes

Yihong Jia^a, Zeid A. ALOthman^b, Rui Liang^c, Shuangshuang Cha^a, Xiaoyong Li^a, Weiyi Ouyang^a, Aquan Zheng^a, Sameh M. Osman^b, Rafael Luque^{d,*}, Yang Sun^{a,**}

^a Department of Applied Chemistry, School of Science, Xi'an Jiaotong University, No. 28, Xianning West Road, Xi'an, 710049, PR China

^b Chemistry Department, College of Science, King Saud University, P.O.Box 2455, Riyadh, 11451, Saudi Arabia

^c School of Resources and Environment, Anhui Agriculture University, No. 130, Changjiang West Road, Hefei, 230036, PR China

^d Departamento de Química Organica, Universidad de Cordoba, Campus de Rabanales, Edificio Marie Curie (C-3), Ctra Nnal IV-A, Km 396, E14014, Cordoba, Spain

ARTICLE INFO

Keywords:

(tartrate-salen)Mn(III)
Immobilization
SBA-15
Asymmetric epoxidation
Enantioselectivity

ABSTRACT

A series of (tartrate-salen)Mn(III) polymer complexes were prepared and immobilized into SBA-15, being subsequently employed as catalysts in the asymmetric epoxidation of alkenes. ¹H NMR, FT-IR, UV-vis, elemental analysis, GPC and ICP-AES demonstrated the successful synthesis of polymer complexes, while powdered XRD, nitrogen physisorption and XPS studies proved the immobilization of polymer complexes into SBA-15. Both homogeneous and heterogeneous catalysis revealed that configurations of major epoxide products were still determined by salen chirality but e.e. values could be improved when tartrate and salen were configurationally identical. Combinations of (*R,R*)-salen with (*R,R*)-tartrate usually offered higher enantioselectivities. SBA-15 was satisfactory supporting material due to the high enantioselectivities and recycling yields obtained. The synthesized SBA-15-supported (tartrate-salen)Mn(III) catalysts showed continuous high enantioselectivities for epoxidation of α -methylstyrene, indicating great prospects for large-scale production.

1. Introduction

Efficient preparation of enantiomerically pure epoxides attracted continuous attention in the fields of both pharmaceutical and material sciences as versatile key blocks for building complex molecules [1,2]. The optical purities of epoxide compounds were determined by the asymmetric epoxidation of alkenes facilitated by various catalysts, which appeared to be an important strategy for academic research and industrial production [3–5]. Atom economy and environmental concerns of this transformation also aroused interests, mainly for large-scale productions [4,5].

In the early years, Sharpless and co-workers established a Ti(IV)/tartrate system that afforded high enantioselectivities in epoxidation of allylic alcohols, a standard transformation in many laboratories around the world [6]. Later, Jacobsen [7] and Katsuki [8] independently developed chiral (salen)Mn(III) complexes (salen, *N,N'*-bis(salicylidene)ethylenediaminato) for epoxidation of unfunctionalized alkenes, where moderate to high enantioselectivities and yields were obtained in conversions of many *cis*- and *tri*-alkenes [7,8]. Furthermore, this catalytic system quickly became very popular in several epoxidation

applications due to some positive properties including synthetic convenience and environmental friendliness, although still needing improvements for certain conversions of *trans*- or terminal alkenes [9]. On the basis of the above progresses, it seemed interesting and significant to test the activity of the combination of tartrate with (salen)Mn(III) complex, where two types of chiralities may show some encouraging synergistic effects in catalytic asymmetric epoxidation of alkenes.

Recycling of (salen)Mn(III) complexes was usually very difficult, and separation of products with (salen)Mn(III) was also inconvenient, actually blocking the road to industrial applications [10]. A large number of endeavors towards heterogenization of (salen)Mn(III) complexes had been carried out in order to overcome this drawback, including dimerization [11] or polymerization of (salen)Mn(III) complexes [12], (salen)Mn(III) being grafted onto polymers [13] and inorganic materials [14] or the use of ionic liquids as supporting materials [15]. However, these strategies were not so successful up to date. Firstly, most polymeric (salen)Mn(III) complexes were still soluble in CH₂Cl₂ or THF, so product separation was still a problem, and the synergistic effects of multiple chiral centers were not completely revealed [16]. Secondly, insufficient accessibility of substrates to metal centers

* Corresponding author at: Department of Applied Chemistry, School of Science, Xi'an Jiaotong University, No. 28, Xianning West Road, Xi'an, 710049, PR China.

** Corresponding author.

E-mail addresses: q62alsor@uco.es (R. Luque), sunyang79@mail.xjtu.edu.cn (Y. Sun).

stemming from supported (salen)Mn(III) catalysts led to reduced catalytic activities and enantioselectivities [16]. Supporting materials may play a key role in catalysis as ligands, so their acid-base properties, steric hindrances, electronic effects, and surface periodicities certainly deserved comprehensive and careful discussions [17]. In general, there is still a big room for exploring new strategies for heterogenization of (salen)Mn(III) complex catalysts.

Currently, immobilization of homogeneous complexes into insoluble solids having ordered structures appeared to be a very promising method for the desing of advanced heterogeneous catalysts. SBA-15 attracted interest from the community for more than one decade as a well-ordered hexagonal mesoporous silicate featuring some advantages as compared to classical MCM-41 including thicker pore wall, larger pores, as well as unique internal connectivity among piled silicate pipes [18]. Its combination with homogeneous catalysts usually showed improved activities than homogeneous counterparts [18].

SBA-15 was also successfully employed as supporting material for several heterogeneous catalysts [19]. In practice, the anchoring of large molecules into SBA-15 internal channels featuring sizes of 5–9 nm looked attractive but difficult [20]. Thus, axial coordination of supports to manganese centers seemed to be another option for holding large (salen)Mn(III) complexes [21], while non-covalent linkages were also tested in supporting (salen)Mn(III) [21]. Furthermore, it was previously supposed that a (salen)Mn(III) polymer complex could be formed and assembled within channels of zeolite using a “ship-in-a-bottle” strategy [22]. Overall, immobilization of (salen)Mn(III) compounds into SBA-15 could create relevant systems for asymmetric epoxidation reactions.

In this work, four chiral (tartrate-salen)Mn(III) polymer complexes were prepared as catalysts for asymmetric epoxidation reactions (Fig. 1). SBA-15 was selected to construct a rigid supporting environment, in which a “ship-in-a-bottle” strategy was employed to assemble (tartrate-salen)Mn(III) into SBA-15. Both homogeneous and heterogeneous catalysts pointed to the presence of synergetic effects among chiral centers stemming from different blocks of catalyst. In addition, sodium hypochlorite was unstable and corrosive, and alternatively some solid oxidants including iodosylbenzene and 3-chloroperoxybenzoic acid were utilized in this work to establish a more sustainable process for the future large-scale applications.

2. Experimental

2.1. Materials

2-*tert*-Butylphenol, tetrabutylammonium bromide (TBAB), paraformaldehyde, *L*-(+)-tartaric acid, *D*-(-)-tartaric acid, sodium *L*-(+)-tartrate dihydrate, sodium *D*-(-)-tartrate dihydrate, styrene, α -methylstyrene, *trans*-stilbene, indene, 1,2-diaminocyclohexane (mixture of isomers), 3-aminopropyltrimethoxysilane (3-APTMS), Pluronic P123 (average M_n , 5800), tetraethyl orthosilicate (TEOS), 3-chloroperoxybenzoic acid (*m*CPBA), inorganic salts, and HPLC-grade solvents were totally purchased from Sigma-Aldrich Corporation without purification. Regular solvents and silica gel of column and thin layer chromatography were provided by local distributors, some sensitive solvents were further purified in our laboratory. 3-*tert*-Butyl-5-chloromethyl-2-hydroxybenzaldehyde [23], (*R,R*)-1,2-diammoniumcyclohexane mono-(+)-tartrate salt [23], (*S,S*)-1,2-diammoniumcyclohexane mono(-)-tartrate salt [23], SBA-15 [24], Mn5 [25], and iodosylbenzene (PhIO) [26] were synthesized according to literature.

2.2. Characterization

^1H NMR were recorded on a Bruker ADVANCE III instrument (400 MHz): spectral width in Hz (SWH) was 8223.6 Hz, dwell time (DW) was 60.8 μs , temperature was 293.0 K. FT-IR data were collected in potassium bromide pellets on a Bruker Tensor 27 spectrometer, wave numbers were ranged from 400 cm^{-1} to 4000 cm^{-1} . UV-vis spectra

were recorded on Shimadzu UV-1800, samples were fixed at 10^{-3} mol L^{-1} in CH_2Cl_2 (Mn content as criteria), wavelength was ranged from 290 nm to 550 nm. ESI-HRMS of positive molecular ions were detected on microTOF-Q II, Bruker. Daltonics equipment. C, H, and N elemental analyses were tested on an Elementar VarioEL III instrument. Metal ion contents were measured by inductively coupled plasma atomic emission spectrometry (ICP-AES) on an ICPE-9000 spectrometer, Shimadzu, according to standard working curve method. Optional rotations were measured on Perkin-Elmer 341 with λ of 587 nm at 25 $^\circ\text{C}$, and values were formatted as absolute rotation $[\alpha]_D^{25}$, where contents of samples were controlled at 0.01 g mL^{-1} in CH_2Cl_2 . The number (M_n)- and weight (M_w)-average molecular weights and polydispersity indices (PDI, M_w/M_n) of four polymeric salen ligands were measured on a gel permeation chromatography (GPC, Waters 1515–2414) equipped with a Styragel HT3 THF column, temperature was 40 $^\circ\text{C}$, eluent was THF, flow rate was 1 mL min^{-1} , which was calibrated by polystyrene standard.

BET surface area, pore volume, pore radius, and pore size distribution were recorded on Micromeritics ASAP 2020, using N_2 adsorption isotherms at 77.35 K, and each sample was degassed at 150 $^\circ\text{C}$ in vacuum before testing. Surface area was calculated on these isotherms using the multi-point Brunauer-Emmett-Teller (BET) method based on adsorption data in the relative pressure P/P_0 ranged from 0.06 to 0.3. Total pore volume was obtained from N_2 adsorbed at $P/P_0 = 0.97$, both pore volume and pore radius were determined using Barrett-Joyner-Halenda (BJH) method. Bulk density of sample was detected on SOTAX TD2 density detector, CAMAG Corporation. Particle size and zeta potential measurements were carried out in CH_2Cl_2 at 298 K on a Zetasizer Nano ZS90 sepctrometer, Malvern. The X-ray diffraction (XRD) patterns of powdered samples were reported on Shimadzu XRD-6000 (Cu- $\text{K}\alpha_1$, λ 1.54059 \AA), and diffraction data were collected when 2θ angles ranged from 4 $^\circ$ to 55 $^\circ$ with 0.02 $^\circ$ intervals. X-ray photoelectron spectroscopy (XPS) were carried out on Kratos Axis Ultra DLD, irradiation source was monochromatic Al $\text{K}\alpha$ X-ray (1486.6 eV). Scanning electron microscopy (SEM) was performed on JSM-6700F, JEOL.

Thin layer chromatography (TLC) was conducted on glass plates coated with GF₂₅₄ silica gel, where coloration was performed in phosphomolybdic acid (PMA)/ethanol (5% mass percent) solution. Both conversion and enantiomeric excess were determined by chiral HPLC analysis, including a Waters chromatograph (system controller: Waters 1525, binary hplc pump; UV-vis detector: Waters 2998, photodiode array detector; UV detection: 242 nm, determined after wavelength scanning between 210 nm and 400 nm), equipped with a Daicel Chiralcel OD-H column (150 mm \times 4.6 mm; 5 μm particle; mobile phase: *n*-hexane / 2-propanol, 97 / 3, v / v; flow rate: 1.0 mL min^{-1} ; column temperature: 300 K; pressure: 5.0 MPa to 7.0 MPa; sample concentration: 1.0 mg mL^{-1} in *n*-hexane; injection: 10 μL).

2.3. Synthesis of chiral dimeric salicylaldehyde (3)

As shown in Scheme 1, 3-*tert*-butyl-5-chloromethyl-2-hydroxybenzaldehyde (1, 3.25 g, 14.4 mmol) and sodium *L*-(+)-tartrate dihydrate (2a, 1.65 g, 7.2 mmol) were combined with dry triethylamine (30 mL) into a round-bottomed flask (250 mL), and the orange solution was heated at 110 $^\circ\text{C}$ for 3 h under vigorous stirring. Small crystals (sodium chloride) gradually precipitated from the purple solution during this procedure. After being cooled down to room temperature, solvent was removed under reduced pressure, and residue was diluted with CH_2Cl_2 (100 mL). Organic layer was thoroughly washed by water (3 \times 50 mL) and brine (3 \times 50 mL), dried over anhydrous Na_2SO_4 , and filtered. After removal of solvent under rotary evaporation, residue was further purified by column chromatography (SiO_2 , 200–300 mesh; petroleum ether / ethyl acetate, 6 / 1, v / v, with a few drops of triethylamine) to afford chiral dimeric salicylaldehyde (3a, yellow sticky solid, 1.49 g, 39 % yield).

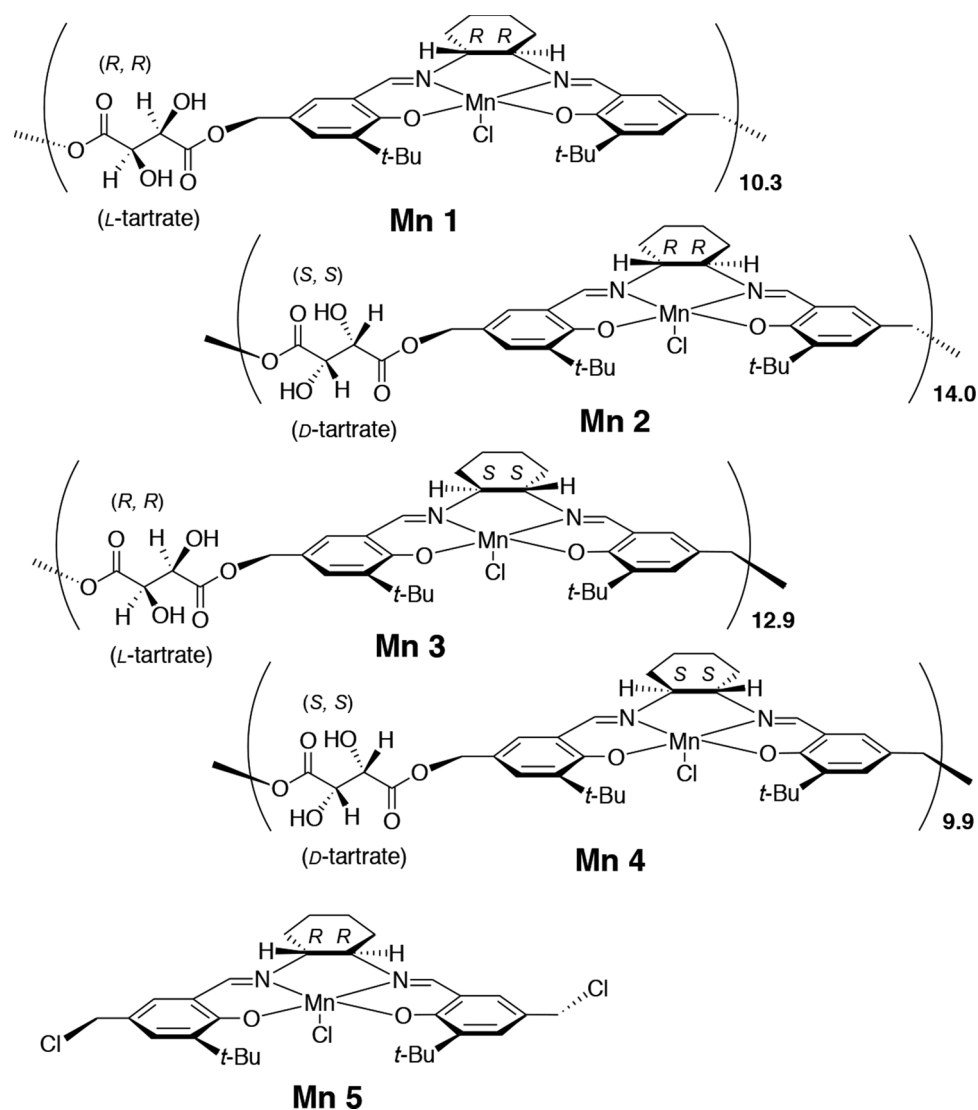


Fig. 1. Configuration illustration of (tartrate-salen)Mn(III) polymer complexes and (salen)Mn(III) monomer complex.

^1H NMR (400 MHz, CDCl_3) δ_{H} , ppm: 1.27 (9H, s, $\text{C}(\text{CH}_3)_3$), 3.95 (4H, s, CH_2 on methylene), 4.55 (2H, s, CH on tartrate), 7.18–7.23 (2H, m, ArH), 7.50–7.61 (2H, m, ArH), 9.85 (2H, s, CHO). FT-IR (KBr) σ , cm^{-1} : 3432 (m, O–H on tartrate), 3398–3280 (br, s, ArO-H), 2939 (s, C–H on methyl), 2856 (s, C–H on methylene), 1719 (vs, C=O stretching on phenyl). ESI-HRMS (positive, m / z): 553.6002 (Calcd. for $[\text{M} + \text{Na}]^+$ 553.5519). $[\alpha]_{\text{D}}^{25} = -65$ (c 0.01 g mL^{-1} , CH_2Cl_2). Ideal formula of 3a is $\text{C}_{28}\text{H}_{34}\text{O}_{10}$. Anal. Calcd.: C, 63.4; H, 6.4. Found: C, 62.8; H, 7.0. Synthesis of 3b was identical to 3a except for replacement of sodium *L*(+)-tartrate dihydrate by sodium *D*(-)-tartrate dihydrate (Sect. A1, Supplementary data).

2.4. Synthesis of chiral ligands (L)

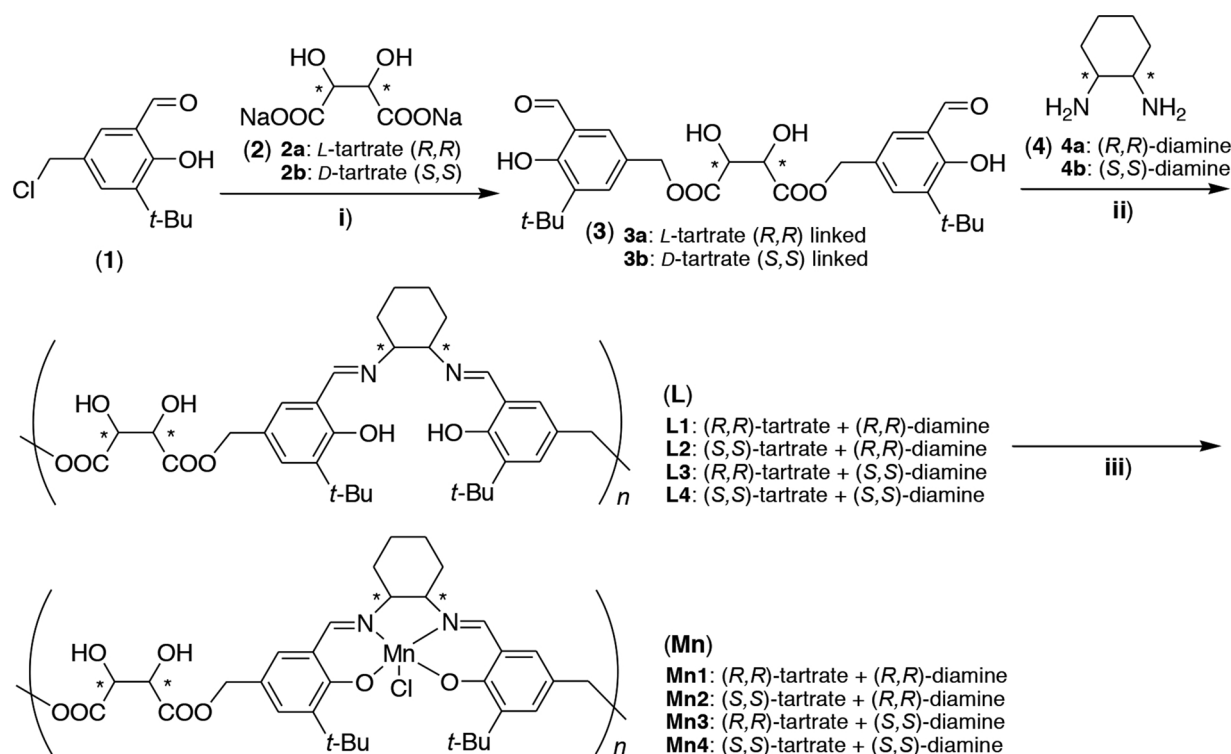
(*R,R*)-1,2-diammoniumcyclohexane mono-(+)-tartrate salt (0.45 g, 1.7 mmol) and anhydrous K_2CO_3 (0.47 g, 3.4 mmol) were combined with distilled water (15 mL) into a round-bottomed flask (250 mL) at room temperature, followed by addition of dry ethanol (6 mL) under vigorous stirring. The cloudy solution was heated at 75°C for 2 h with stirring and then cooled to room temperature. As shown in Scheme 1, free diamine was carefully extracted by CH_2Cl_2 (4 \times 5 mL), and then slowly added to a pre-prepared ethanol solution of 3a (0.9 g, 1.7 mmol, in 20 mL) at room temperature under stirring. The orange solution was refluxed at 80°C for 3 h under vigorous stirring. After removal of

solvent under reduced pressure, the crude product was dissolved in CH_2Cl_2 (30 mL), and organic layer was washed with distilled water (50 mL), brine (50 mL), dried over anhydrous Na_2SO_4 , and filtered. Solvent was removed by rotary evaporation, and L1 was obtained as yellow sticky solid (0.96 g).

^1H NMR (400 MHz, CDCl_3) δ_{H} , ppm: 1.41 (9H, s, $\text{C}(\text{CH}_3)_3$), 1.40–1.56 (8H, m, CH_2 on cyclohexyl), 2.33 (2H, s, CH on cyclohexyl), 3.93 (4H, s, CH_2 on methylene), 4.53 (2H, s, CH on tartrate), 7.40–7.44 (2H, m, ArH), 7.50–7.55 (2H, m, ArH), 9.88 (2H, s, CHN). FT-IR (KBr) σ , cm^{-1} : 3442 (br, s, ArO-H , O–H on tartrate, overlapped), 2958 and 2867 (m, C–H on methyl), 2930 (m, C–H on methylene), 1772 (w, tartrate), 1649 (s, C = N), 1559 (w, C–O), 1267 (w, Ar-OH). $[\alpha]_{\text{D}}^{25} = -116$ (c 0.01 g mL^{-1} , CH_2Cl_2). $M_n = 6262$, $M_w = 13150$, PDI (M_w/M_n) = 2.1. Based on M_n , number of tartrate-salen monomers was 10.3, then ideal formula of L1 was deduced as $(\text{C}_4\text{H}_4\text{O}_6\text{:C}_{30}\text{H}_{40}\text{O}_2\text{N}_2)_{10.3}$. Anal. Calcd.: C, 67.1; H, 7.2; N, 4.6. Found: C, 66.8; H, 6.7; N, 5.5. Synthesis of L2, L3, and L4 was identical to L1 except for substitution of chiral tartrate and diamine counterparts (Sect. A2, Supplementary data).

2.5. Synthesis of (tartrate-salen)Mn(III) polymer complexes (Mn)

L1 (0.81 g) and $\text{Mn}(\text{OAc})_2\cdot 4\text{H}_2\text{O}$ (0.62 g, 2.55 mmol) were combined into anhydrous ethanol (10 mL) into a round-bottomed flask (100 mL), and the resulting mixture was refluxed at 75°C for 3 h under nitrogen



Scheme 1. Synthesis of (tartrate-salen)Mn(III) polymer complexes. Reagents and conditions: i) triethylamine, 110 °C, 3 h; ii) chiral diamine extraction first: (R,R)-1,2-diammoniumcyclohexane mono-(+)-tartrate salt or (S,S)-counterpart, K_2CO_3 , ethanol / water, 75 °C, 2 h; polymerization second, ethanol, 80 °C, 3 h; iii) Mn(OAc) $_2$ ·4H $_2$ O, anhydrous ethanol, N $_2$ protection, 75 °C, 3 h; LiCl·H $_2$ O, open system, 75 °C, 1 h.

protection. Protection was removed and LiCl·H $_2$ O (0.46 g, 7.65 mmol) was introduced. The solution was further stirred at 75 °C for an hour in air, then total solvent was removed by rotary-evaporation and brown powders were collected and thoroughly washed by distilled water (3 × 30 mL), then Mn1 was obtained as brown powders (0.76 g).

FT-IR (KBr) σ , cm $^{-1}$: 3433 (br, s, O-H on tartrate, H-OH, overlapped), 2957 and 2868 (m, C-H on methyl), 2930 (m, C-H on methylene), 1741 (w, tartrate), 1618 (s, C = N), 1544 (w, C-O), 1268 (w, Ar-OMn), 567 (w, Mn-O). $[\alpha]_D^{25} = +129$ (c 0.01 g mL $^{-1}$, CH $_2$ Cl $_2$). According to L1, ideal formula of Mn1 was summarized as (C $_4$ H $_4$ O $_6$ ·C $_30$ H $_38$ O $_2$ N $_2$ MnCl·2H $_2$ O) $_{10.3}$. Anal. Calcd.: C, 55.7; H, 6.2; N, 3.8. Found: C, 56.3; H, 6.1; N, 4.5. Mn $^{3+}$ was 1.10 mmol g $^{-1}$ by ICP-AES. Synthesis of other polymer complexes (Mn2, Mn3, Mn4, Scheme 1) were identical to Mn1 in the presence of corresponding ligands (Sect. A3, Supplementary data).

2.6. Synthesis of SBA-15-supported (tartrate-salen)Mn(III) polymer complexes (Mnx@S and Mnx@aS, x = 1, 2, 3, 4)

SBA-15-supported (tartrate-salen)Mn(III) complexes were synthesized according to a “ship-in-a-bottle” strategy, as shown in Scheme 2. The (R,R)-1,2-diammoniumcyclohexane mono-(+)-tartrate salt (0.24 g, 0.89 mmol) and anhydrous K $_2$ CO $_3$ (0.25 g, 1.78 mmol) were combined with distilled water (15 mL) into a round-bottomed flask (100 mL) at room temperature, followed by addition of dry ethanol (6 mL) under vigorous stirring. The cloudy solution was heated at 80 °C for 2 h with stirring and then cooled to room temperature. Free diamine was carefully extracted by CH $_2$ Cl $_2$ (2 × 5 mL). In another round-bottomed flask (100 mL), 3a (0.47 g, 0.89 mmol) and SBA-15 (1.0 g) were combined into anhydrous ethanol (10 mL) under vigorous stirring at room temperature for 1 h, the CH $_2$ Cl $_2$ layer containing diamine was added dropwise, and the suspension was stirred at 50 °C for 3 h. Mn(OAc) $_2$ ·4H $_2$ O (0.22 g, 0.89 mmol) was introduced and suspension was further refluxed at 50 °C under nitrogen protection for 3 h. Protection

was removed and LiCl·H $_2$ O (0.23 g, 3.82 mmol) was added, suspension was continuously stirred at 50 °C for 1 h in air. Herein, the dark mixture was divided into two equal portions. For the first portion, solvent was removed by rotary-evaporation and brown powders (Mn1@S, 0.45 g) were collected after washing with distilled water (3 × 5 mL) and anhydrous ethanol (3 × 5 mL).

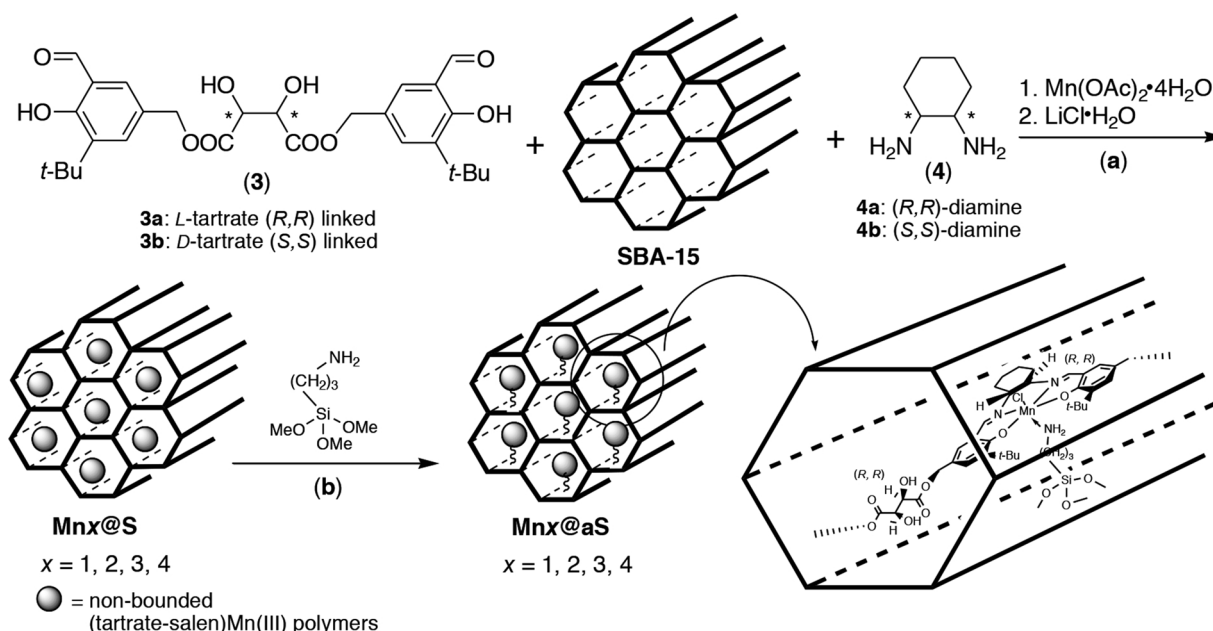
FT-IR (KBr) σ , cm $^{-1}$: 3509 (br, m, SiO-H), 3447 (br, m, O-H on tartrate), 3325 (br, m, H-OH), 2957 and 2870 (both w, C-H on methyl), 2920 (w, C-H on methylene), 1766 (w, tartrate), 1622 (m, C = N), 1558 (m, C-O on tartrate), 1078 (s, Si-O), and 799 (w, Si-O). Mn $^{3+}$ is 0.17 mmol g $^{-1}$ determined by ICP-AES. Mnx@S (x = 2, 3, 4) were prepared according to the same procedure when corresponding bis-aldehyde and diamine were loaded (Sect. A4, Supplementary data).

3-APTMS (0.2 g, 1.14 mmol) and anhydrous toluene (10 mL) were introduced, and mixture was stirred at 50 °C for 6 h. After removal of solvent under reduced pressure, residue was carefully washed with distilled water (3 × 5 mL) and anhydrous ethanol (3 × 5 mL), then filtrated, and Mn1@aS was obtained as brown powders (0.61 g).

FT-IR (KBr) σ , cm $^{-1}$: 2956 and 2875 (both m, C-H on methyl), 2916 (m, C-H on methylene), 1759 (w, tartrate), 1625 (w, C = N), 1558 (m, C-O on tartrate), 1079 (s, Si-O), and 800 (w, Si-O). Mn $^{3+}$ is 0.16 mmol g $^{-1}$ determined by ICP-AES. Mnx@aS (x = 2, 3, 4) were prepared according to the same procedure when corresponding bis-aldehyde and diamine were loaded from the very beginning of this section (Sect. A4, Supplementary data).

2.7. Catalytic reactions

Alkene (1 mmol), catalyst (0.03 mmol Mn, 3 mol% on alkene, also changed as shown in Table 3), PhIO (or *m*-CPBA, 1.2 mmol) and NH $_4$ OAc (co-catalyst, 0.12 mmol) were dissolved in CH $_2$ Cl $_2$ (5 mL, same volume for other solvents) and then placed into a round-bottomed flask (100 mL) at 0 °C. The mixture was vigorously stirred and monitored by TLC in combination with PMA coloration (petroleum ether / CH $_2$ Cl $_2$, 2



Scheme 2. Synthesis of heterogeneous (tartrate-salen)Mn(III) polymer complexes. Reagents and conditions: (a) compound 3 and SBA-15 mixing firstly: anhydrous ethanol, 1 h, room temperature; chiral diamine extraction secondly: tartrate salt of chiral diamine, K_2CO_3 , H_2O / EtOH, 80 °C, 2 h; polymerization next: anhydrous ethanol/ CH_2Cl_2 , 50 °C, 3 h; metalation at last: $Mn(OAc)_2 \cdot 4H_2O$, N_2 protection, 50 °C, 3 h, then $LiCl \cdot H_2O$, open system, 50 °C, 1 h. (b) anhydrous ethanol / CH_2Cl_2 / toluene, 50 °C, 6 h.

/ 1, v/v ; R_f of styrene, α -methylstyrene, *trans*-stilbene, and indene: 0.89, 0.86, 0.72, 0.75; R_f of epoxides for above alkenes: 0.26, 0.23, 0.36, and 0.32 correspondingly).

After 6 h, the mixture was completely concentrated under reduced pressure (only omitted for entry 6 of Table 4, direct extraction instead), the residue was extracted by *n*-hexane (3×5 mL), and the left solid catalysts were recovered and reloaded with consumables for recycling. Hexane layer was concentrated under reduced pressure, and crude product was purified by a short column chromatography (alkaline aluminum oxide; petroleum ether / CH_2Cl_2 , 2 / 1, v/v , with a few drops of triethylamine), and then both conversion and e.e. value were determined by chiral HPLC.

3. Results and discussion

3.1. Design and synthesis of catalysts

Design of (tartrate-salen)Mn(III) polymer complexes was a rational combination of different chiral sources for one catalytic target. When *L*- and *D*-tartrate were combined with (*R,R*)- or (*S,S*)-1,2-diammoniumcyclohexane, four polymer complexes (Mnx , $x = 1, 2, 3, 4$) were obtained with short-range ordering (Fig. 1). The synthetic route of Mnx ($x = 1, 2, 3, 4$) were summarized in Scheme 1. First of all, the esterification of 3-*tert*-butyl-5-chloromethyl-2-hydroxybenzaldehyde with sodium tartrate dihydrate could be accomplished in acceptable yields as long as anhydrous triethylamine were employed as both base and solvent. Chiral diamines should be extracted from alkaline solution before its polymerization with bis-aldehyde (Scheme 1).

Probably due to limited pore size in SBA-15 [27], direct immobilization of large polymers such as $Mn1$ into internal channels of SBA-15 seemed a little difficult. In practice, $Mn1$ (0.2 g) and SBA-15 (0.4 g, as shown in Section 2.6) had been vigorously stirred in anhydrous ethanol at 60 °C for 12 h, then filtered and solids were collected after washing by anhydrous ethanol (3×5 mL). Mn^{3+} in solids was 4.9×10^{-3} mmol g^{-1} tested by ICP-AES, probably owing to trace of physically adsorbed Mn catalyst. Therefore, a “ship-in-a-bottle” strategy was put forward in Scheme 2, including self-assembling of $Mn1$ inside SBA-15 and subsequent coordination of amino groups with Mn centers.

3.2. FT-IR spectroscopy

FT-IR spectra of $L1$, $Mn1$, SBA-15, $Mn1@S$, and $Mn1@aS$ were shown in Fig. S1 (Sect. A5, Supplementary data). FT-IR of $L1$ (a, Fig. S1) showed characteristic vibration bands at 3442 (ArO-H, O-H on tartrate, overlapped), 2958 and 2867 (C-H on methyl), 2930 (C-H on methylene), 1772 (tartrate), 1649 (C = N), 1559 (C-O), and 1267 (Ar-OH) cm^{-1} , while $Mn1$ exhibited corresponding vibrations at 3433, 2957 and 2868, 2930, 1741, 1618, 1544, and 1268 (Ar-OMn) cm^{-1} , together with a new vibration of Mn-O stretching at 567 cm^{-1} (b, Fig. S1). The red shift was observed on C = N stretching from 1649 to 1618 cm^{-1} (b vs. a, Fig. S1), being ascribed to the coordination of nitrogen to Mn^{3+} that reduced electron density on imine [28]. In particular, the red shift of tartrate from 1772 to 1741 cm^{-1} and that of C-O on tartrate from 1559 to 1544 cm^{-1} could be rationalized as coordination of tartrate unit to Mn^{3+} center (b vs. a, Fig. S1), probably indicating a curved configuration of $Mn1$ instead of a linear one.

Pure SBA-15 exhibited a simpler FT-IR spectrum, with typical bands at 3517 (SiO-H), 1086 and 809 (Si-O) cm^{-1} (c, Fig. S1). After “ship-in-a-bottle” immobilization, $Mn1$ was caged into SBA-15 channels, and $Mn1@S$ showed characteristic vibrations at 3509 (SiO-H), 3447 (O-H on tartrate), 3325 (H-OH), 2957 and 2870 (C-H on methyl), 2920 (C-H on methylene), 1766 (tartrate), 1622 (C = N), 1558 (C-O on tartrate), 1078 and 799 (Si-O) cm^{-1} (d, Fig. S1), having higher wave numbers for ester stretching of tartrate, C = N, as well as C-O on tartrate as compared to $Mn1$, supposing coordination of tartrate with Mn^{3+} centers was limited due to hindrance of SBA-15 channels. $Mn1@aS$ showed sharply declined SiO-H stretching than $Mn1@S$ (e vs. d, Fig. S1), which witnessed coupling of 3-APTMS with inner surface of SBA-15, while other bands at 2956 and 2875 (C-H on methyl), 2916 (C-H on methylene), 1759 (tartrate), 1625 (C = N), 1558 (C-O on tartrate), 1079 and 800 (Si-O) cm^{-1} (e, Fig. S1) suggested $Mn1$ was entirely attached to SBA-15. In addition, $Mn1@aS$ showed a higher C=N stretching (1625 cm^{-1}) than $Mn1$ (1618 cm^{-1}) and $Mn1@S$ (1622 cm^{-1}) that described characteristics of axial coordination (g vs. d and f, Fig. S1) [29].

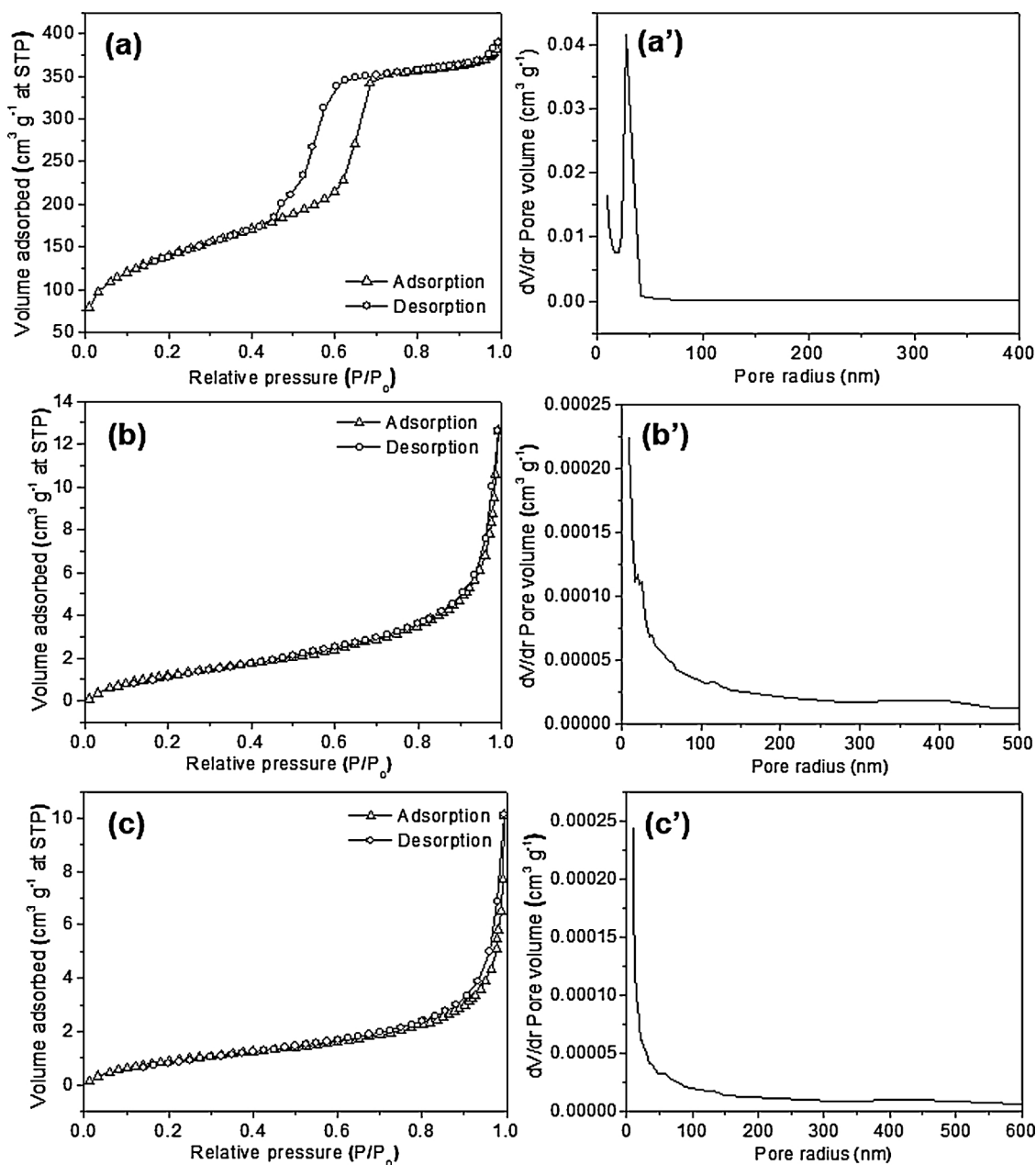


Fig. 2. N₂ adsorption-desorption isotherms and pore size distributions of SBA-15 (a and a'), Mn1@S (b and b') and Mn1@aS (c and c').

Table 1
Physicochemical properties of synthetic samples.

Sample	S_{BET}^a	PV^b	PR^c	ρ^d	d_s^e	d_w^f	ζ^g
SBA-15	482	5.9×10^{-1}	26.2	0.81	15.3	36.7	-19.67
Mn1@S	< 10	1.9×10^{-2}	66.8	0.63	1790.1	188.2	-4.70
Mn1@aS	< 5	1.5×10^{-2}	79.7	0.62	2601.4	606.3	-3.97

^a Surface area ($\text{m}^2 \text{g}^{-1}$) determined by BET method based on N₂ adsorption.

^b Pore volume ($\text{cm}^3 \text{g}^{-1}$), BJH method on N₂ adsorption.

^c Pore radius (nm), BJH method on N₂ adsorption.

^d Bulk density (g cm^{-3}).

^e Crystallite size (nm) based on BET surface area: $d_s = 6/(S_{\text{BET}}\rho)$, ρ bulk density.

^f Diameter of particle in CH₂Cl₂ (nm).

^g Zeta potential of particle in CH₂Cl₂ (mV).

3.3. UV-vis spectroscopy

Fig. S2 showed UV-vis spectra of L1, Mn1, Mn1@S, and Mn1@aS (Sect. A6, Supplementary data). In spectrum of L1 (a, Fig. S2), both 292 and 340 nm could be assigned to charge transfer transition of salen ligand [25], while Mn1 exhibited corresponding responses at 294 and 347 nm (b, Fig. S2), bearing two small shifts due to coordination of manganese [25]. Both Mn1@S and Mn1@aS showed observable shifts in comparison with Mn1 (d vs. b, and e vs. b, Fig. S2), which confirmed the corresponding attachment.

3.4. Nitrogen physisorption

SBA-15 had a type IV isotherm with a characteristic hysteresis loop, bearing a highly regular pore size distribution (a and a', Fig. 2), characteristic of a mesoporous structure [30]. Neither Mn1@S nor Mn1@aS could maintain such a fine structure, and both showed type II isotherms (b and c, Fig. 2) associated with sharply decreased surface areas and

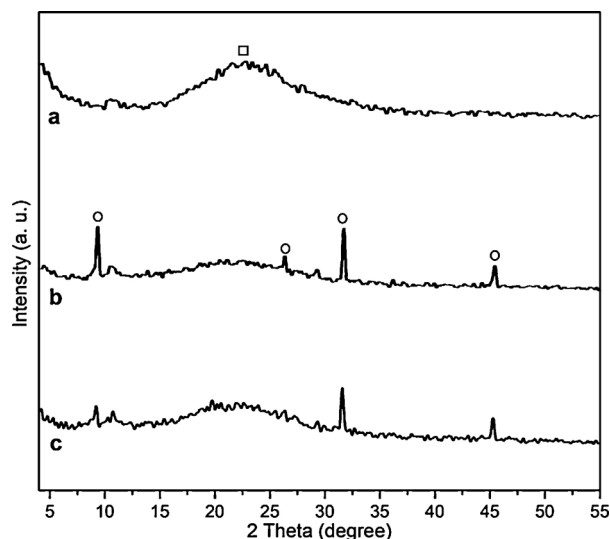


Fig. 3. Powdered XRD patterns of SBA-15 (a), Mn1@S (b), and Mn1@aS (c).

pore volumes of essentially non-porous materials (Table 1).

3.5. Powdered XRD

Fig. 3 showed powdered XRD spectra SBA-15, Mn1@S, and Mn1@aS. Pure SBA-15 showed no well-resolved peaks at range of 4° to 55° , and only a noncrystalline diffraction was observed at 22.7° (2θ) along with 3.90 \AA (cube, a, Fig. 3). After immobilization of Mn1, Mn1@S turned out to be more crystallized, bearing four 2θ peaks centered at 9.1° (9.60 \AA), 26.2° (3.39 \AA), 31.6° (2.82 \AA), as well as 45.3° (1.99 \AA) (circles, b, Fig. 3), and original noncrystalline peak at 22.7° (3.90 \AA) of SBA-15 was quickly attenuated (b vs. a, Fig. 3). The first two diffractions of Mn1@aS at 9.2° and 26.3° unambiguously degraded in comparison with those found in Mn1@S (c vs. b, Fig. 3), possibly because 3-APTMS compressed both Mn1 and SBA-15 and made material less crystallized. In general, SBA-15 was sealed by either Mn1 or 3-APTMS, and both Mn1@S and Mn1@aS should have a denser structure than SBA-15, naturally leading to much smaller surface areas (Table 1).

3.6. Chemical composition

Elemental analysis, metal contents, and molar ratio of N to Mn were summarized in Table 2, affording a macroscopic evaluation on chemical composition of synthetic samples. Pure SBA-15 contained a trace amount of hydrogen and marginal carbon content, indicating most of organic template had been removed after calcination, but higher contents of carbon and hydrogen in Mn1@S confirmed an effective immobilization (Table 2). Introduction of 3-APTMS could not improve Mn

Table 2
Chemical composition data of synthetic samples.

Sample	Elemental analysis ^a			Mn ^b	N / Mn ^c
	C	H	N		
L1	66.8 (67.1)	6.7 (7.2)	5.5 (4.6)	–	–
Mn1	56.3 (55.7)	6.1 (6.2)	4.5 (3.8)	1.10 (1.36)	2.9
SBA-15	4.1	1.1	–	–	–
Mn1@S	19.2	7.8	0.6	0.17	2.5
Mn1@aS	26.6	19.9	4.6	0.16	20.5

^a Weight percentage (wt%), data shown in parentheses were calculated values.

^b Determined by ICP-AES (mmol g^{-1}), data shown in parentheses were calculated values.

^c Molar ratio of N to Mn, deduced from N% found and Mn content detected.

Table 3
Binding energies and surface atomic compositions from synthetic samples.

Sample	C (1 s)	Si (2p)	N (1 s)	Mn (2p)
SBA-15	282.0 (21.3)	101.0 (34.5)	–	–
Mn1@S	282.0 (53.4)	100.0 (18.5)	–	639.0 (0.3)
Mn1@aS	282.0 (78.5)	100.0 (5.9)	396.0 (1.5)	639.0 (0.2)

^a Binding energy (eV), together with atomic percentage (at%) in parentheses.

Table 4
Enantioselective epoxidation of styrene for optimization of catalytic conditions.

Entry ^a	Cat. Loading (mol%) ^b	Solvent ^c	Conversion ^d (%)	E.e. ^e (%)	TOF ^f
1	3	Acetone	22	16 (R)	1.2
2	3	Diethyl ether	36	13 (R)	2.0
3	3	Acetonitrile	33	3 (R)	1.8
4	3	<i>n</i> -Hexane	40	19 (R)	2.2
5	3	Ethanol	21	11 (R)	1.1
6	3	Water	8	7 (R)	0.8
7	3	Dichloromethane	11	38 (R)	0.6
8	1.5	Dichloromethane	10	19 (R)	0.5
9	6	Dichloromethane	26	21 (R)	1.4

^a Reaction conditions: styrene (1 mmol), NH_4OAc (co-catalyst, 0.12 mmol), PhIO (1 mmol), solvent (5 mL), T (273 K), time (6 h).

^b Mn1 loading, based on the molar ratio of manganese content to original alkene, formatted as mol%.

^c Solvent volume fixed at 5 mL for all entries.

^d Conversion, molar ratio of epoxide products to original alkene, determined by HPLC over a Daicel Chiralcel OD-H column at 300 K.

^e Enantiomeric excess, determined by HPLC over Daicel Chiralcel OD-H column. Major epoxide enantiomer for all entries of this table was (R)-styrene oxide, as emphasized in parenthesis, based on comparison with literature data [32] (Sect. A7, Supplementary data).

^f Turnover frequency, $\text{mol}_{\text{product}} \text{mol}_{\text{Mn}}^{-1} (\text{6 h})^{-1}$, h^{-1} as unit.

content, but the highest molar ratio of N/Mn illustrated amino groups were also excessive enough to link with all manganese centers (Table 2).

3.7. X-ray photoelectron spectroscopy

Binding energy and surface atomic composition of synthetic products were summarized in Table 3. Carbon molar ratios on surfaces of SBA-15, Mn1@S, and Mn1@aS were increased, but corresponding Si contents decreased (Table 3), certifying package of Mn1 or 3-APTMS around SBA-15. In Fig. 4, Mn 2p_{3/2} and Mn 2p_{1/2} binding energies of Mn1@S were 638.7 eV and 650.6 eV respectively, higher than those of

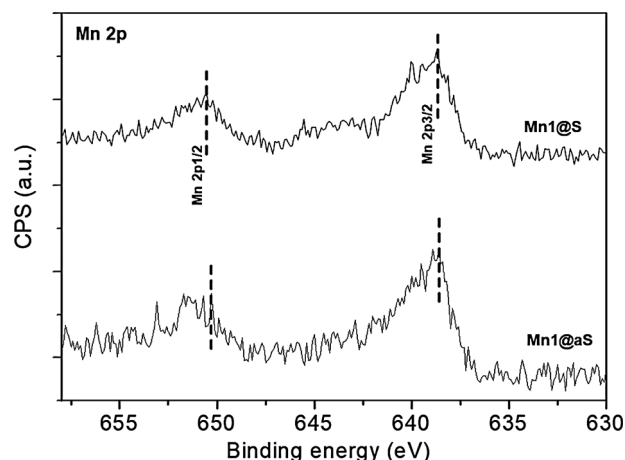


Fig. 4. XPS measurements of Mn 2p regions for Mn1@S and Mn1@aS.

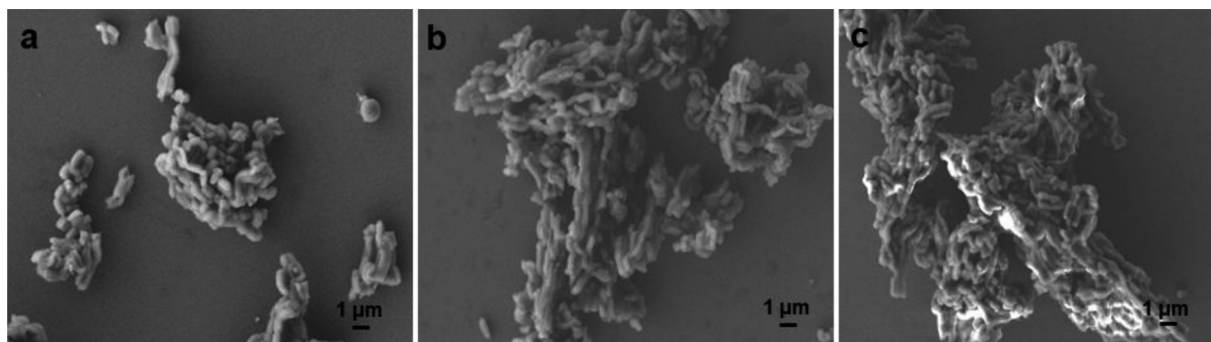


Fig. 5. SEM images of (a) SBA-15, (b) Mn1@S and (c) Mn1@aS.

Mn1@aS at 638.6 eV and 650.3 eV, supposing coordination of nitrogen decrease density of positive charges on Mn^{3+} centers [31].

3.8. Scanning electron microscopy

Size and morphology of SBA-15, Mn1@S, and Mn1@aS were characterized by scanning electron microscopy, as shown in Fig. 5. The morphologies of all synthetic samples looked similar because the SBA-15 rods were kept well, but apparently the more modification was, the denser sample particles became (a–c, Fig. 5). Therefore, the “ship-in-a-bottle” strategy carried out in this study would not only construct manganese complexes inside channels of SBA-15, but bind rods of SBA-15 that finally led to a decreased surface area as shown in Table 1.

3.9. Optimization of catalytic conditions

(tartrate-salen)Mn(III) polymer complexes Mn1 to Mn4 were soluble in dichloromethane, acetone, diethyl ether, and acetonitrile, less soluble in *n*-hexane and ethanol, but immiscible in water. In order for optimization of reaction conditions, asymmetric epoxidation of styrene catalyzed by Mn1 was conducted at 0 °C with PhIO selected as oxidant.

Catalytic results are summarized in Table 4. Conversion, enantioselectivity as well as turnover frequency appeared to be highly solvent dependent. Mn1 was practically immiscible with water, it aggregated and deposited on the flask during catalysis, so interaction between Mn1 and substrate at molecular level was poor, conversion and enantioselectivity were limited (entry 6, Table 4). Ethanol, another protic solvent, was not appropriate either, although it showed some improvement than water (entries 5 vs. 6). Pronounced enantioselectivity and acceptable conversion came from the reactions facilitated by some non-protic solvents such as dichloromethane or *n*-hexane (entries 7 and 4, Table 4), supposedly these non-protic solvents could promote S_N2 reactions including epoxidation [33]. On the other hand, catalyst loading also played an important role in both conversion and enantioselectivity. Although the largest catalyst loading (6 mol%) afforded the highest conversion (26 %) among three dichloromethane facilitated reactions (entries 9 vs. 7 and 8), but its e.e. was lower than that found in 3 mol% (entries 7 vs. 9). Dichloromethane and 3 mol% of catalyst loading were selected as optimum for subsequent reactions.

3.10. Catalysis of polymer complexes and monomer complex

Polymer complexes Mn1 to Mn4 were selected as catalyst for asymmetric epoxidation of four unfunctionalized alkenes including styrene, α -methylstyrene, *trans*-stilbene, and indene. The monomeric Mn5 was also tested as comparative criteria in order to disclose the roles of tartrate linkers in enantioselectivity or reactivity. Catalytic results were listed in Table 5.

In general, all homogeneous catalytic reactions proceeded smoothly, and all reactions would be accomplished within 6 h under monitoring of TLC in conjunction with PMA coloration. At 0 °C, PhIO

was completely immiscible with CH_2Cl_2 , so the oxygen transfer slowly occurred on surface of PhIO, which was able to explain comparatively higher e.e. values (in most cases) but less abundant conversions found in PhIO facilitated reactions that were quite different with those in *m*CPBA oxidized ones (entries 1 vs. 2, 7 vs. 8, 13 vs. 14, 19 vs. 20, Table 5).

Combination of (*R,R*)-salen with (*R,R*)-tartrate (Mn1) gave the best enantioselectivity as well as acceptable conversion in asymmetric epoxidation of styrene (entry 1, Table 5), but its enantiomer (Mn4) could not afford rivaled data (entries 5 vs. 1, Table 5). And interestingly, Mn1 showed much better e.e. than Mn2, suggesting enantioselectivity would be improved when both tartrate linker and salen had the same (*R,R*)-configurations (entries 1 vs. 3, Table 5). In addition, chiral induction of Mn1 appeared to be more prospective than Mn5 too (entries 1 vs. 6, Table 5), which further confirmed the conjunction of (*R,R*)-tartrate with (*R,R*)-salen in epoxidation of styrene. Taking into account red shift of tartrate found in FT-IR of L1 and Mn1 (a and b, Fig. S1), all these catalytic results probably emphasized chiral tartrate should take part in chiral induction through its coordination with manganese center. Nevertheless, configuration of major styrene oxides was still determined by salen chirality (entries 1–3, 6 vs. 4–5, Table 5).

Configurations of major epoxides for α -methylstyrene were persistent in the presence of Mn1 to Mn5 (entries 7–12, Table 5). However, Mn1, Mn2, and Mn5 showed considerably higher e.e. values and moderate to high conversions for asymmetric epoxidation of α -methylstyrene (entries 7, 9, and 12, Table 5), unambiguously emphasizing the dominant role of (*R,R*)-salen in chiral configuration determination. Furthermore, catalytic results of (*R,R*)-salen associated with (*S,S*)-tartrate (Mn2, entry 9, Table 5) were comparable to the chiral sugar moiety-modified (salen)Mn(III) system [35]. The epoxidation of indene gave excellent e.e. values, satisfactory conversions along with good TOFs when salen and tartrate were configurationally identical (entries 19 and 23, Table 5). But *trans*-stilbene was a tough substrate because neither polymer complexes (Mn1 to Mn4) nor monomer Mn5 could promote chiral induction, and indeed no e.e. values higher than 40 % was observed in all rounds (entries 13–18, Table 5).

At homogeneous level, Mn5 exhibited a superior performance as compared to polymer complexes in the cases of α -methylstyrene (entry 12, Table 5) and *trans*-stilbene (entry 18, Table 5). Mn1 showed comparatively higher e.e. values and acceptable to good conversions for styrene (entry 1, Table 5), α -methylstyrene (entry 7, Table 5), and indene (entry 19, Table 5), Mn4 had a nice performance in epoxidation of indene too (entry 23, Table 5), which both proclaimed the importance of uniform configuration distributed between salen and tartrate.

3.11. Catalysis of SBA-15-supported (tartrate-salen)Mn(III)

SBA-15 provided a porous and curved environment for immobilizing (tartrate-salen)Mn(III) polymer complexes, where “ship-in-a-bottle” strategy had been employed to functionalize this material. Based on catalytic inertness of SBA-15 (entry 1, Table 6), successful

Table 5
Enantioselective epoxidation of unfunctionalized alkenes catalyzed by Mn1-Mn5.

Entry ^a	Alkene	Product	Catalyst ^b	Oxidant ^c	Conv. ^d (%)	E.e. ^e (%)	TOF ^f
1 ^a			Mn1	PhIO	11	38 (R)	0.6
2			Mn1	<i>m</i> CPBA	77	12 (R)	4.2
3			Mn2	PhIO	25	16 (R)	1.3
4			Mn3	PhIO	19	36 (S)	1.0
5			Mn4	PhIO	26	21 (S)	1.4
6			Mn5	PhIO	67	30 (R)	3.7
7			Mn1	PhIO	78	49 (R)	4.3
8			Mn1	<i>m</i> CPBA	80	10 (R)	4.4
9			Mn2	PhIO	81	61 (R)	4.5
10			Mn3	PhIO	17	9 (R)	0.9
11			Mn4	PhIO	32	8 (R)	1.7
12			Mn5	PhIO	22	77 (R)	1.2
13			Mn1	PhIO	54	5 (R,R)	3.0
14			Mn1	<i>m</i> CPBA	55	10 (R,R)	3.0
15			Mn2	PhIO	31	20 (R,R)	1.7
16			Mn3	PhIO	41	5 (S,S)	2.2
17			Mn4	PhIO	25	11 (S,S)	1.3
18			Mn5	PhIO	92	33 (R,R)	5.1
19			Mn1	PhIO	36	67 (1S,2R)	2.0
20			Mn1	<i>m</i> CPBA	61	55 (1S,2R)	3.3
21			Mn2	PhIO	9	26 (1S,2R)	0.5
22			Mn3	PhIO	100	44 (1R,2S)	5.5
23			Mn4	PhIO	100	78 (1R,2S)	5.5
24			Mn5	PhIO	98	39 (1S,2R)	5.4

^a Reaction conditions: alkene (1 mmol), NH₄OAc (co-catalyst, 0.12 mmol), CH₂Cl₂ (5 mL), *T* (273 K), time (6 h). Entry 1 in this table was identical to entry 7 of Table 4.

^b Catalyst loading, based on molar ratio of manganese content to original alkene, fixed at 3 mol%.

^c PhIO or *m*CPBA, 1 mmol.

^d Same as shown in Table 4.

^e Same as shown in Table 4 including separation conditions and literature data for styrene oxide [32]. In addition, major epoxide enantiomers of α -methylstyrene oxide [32], *trans*-stilbene oxide [32], and indene oxide [34] were determined by the same chiral HPLC, after comparison with literatures (Sect. A7, Supplementary data).

^f Same as shown in Table 4.

recycling of Mn1@S for styrene epoxidation might come from rigid fixation of Mn1 inside SBA-15 (entry 2, Table 6) despite the non porous nature of the final material, with particular regards to the restriction of folding or spooling of salen units that would weaken the formation active Mn(V)-oxo intermediates [36]. But the role of axial coordination to Mn³⁺ with nitrogen was not so clear in the cases of styrene, the results for Mn1@aS and Mn4@aS looked negative (entries 3 vs. 2, 9 vs. 8, Table 6). *Trans*-stilbene was still a tough substrate, SBA-15-supported Mn2, Mn3 and Mn4 almost led to racemic products (entries 20, 22, 24, Table 6), and Mn1@aS as well as Mn1@aS could only afford 15 % e.e. values (entries 18–19, Table 6). Probably low enantioselectivity in epoxidation of *trans*-stilbene was highly dependent on its transition states [36], influence of present supporting material seemed to be less effective.

Satisfactory e.e. values and acceptable to high conversions were obtained in epoxidation of α -methylstyrene (entries 10 and 11, Table 6), where Mn1@aS afforded a 92 % e.e. combined with 44 % conversion after five cycles (entry 11, Table 6). Another encouraging instance was application of Mn4@aS in epoxidation of indene that afforded a 99 % e.e. with 78 % conversion in fresh cycle, and a 56 % e.e. with 100 % conversion after five uses (entry 33, Table 6). Hitherto, based on a systematic analysis of catalytic results in Tables 5 and 6, immobilization of Mn1 into SBA-15 could show pronounced and stable results for most substrates.

4. Conclusions

This research comprehensively studied chiral synergetic effects on a series of novel (tartrate-salen)Mn(III) polymer complexes through asymmetric epoxidation reactions of unfunctionalized alkenes at both homogeneous and heterogeneous levels. Intermediates and products were fully characterized that proved synthetic routes available. Further

testified by other characterizations such as nitrogen physisorption and powdered XRD, manganese polymer complexes had been dispersed into SBA-15 materials. Both homogeneous and heterogeneous catalyses demonstrated the improved enantioselectivity could be accomplished in case tartrate and salen were configurationally identical, and polymer complex Mn1, a combination of (*R,R*)-tartrate with (*R,R*)-(salen)Mn(III), along with its heterogeneous catalysts in particular, should have the best catalytic performance including chiral induction, activity and stability. Moreover, α -methylstyrene and indene were appropriate substrates in this system, but not *trans*-stilbene and styrene. At last, some results were highly potential in large-scale production to afford optically pure α -methylstyrene oxide and indene oxide.

Declaration of Competing Interest

The authors declare that they have no known competing financial interests or personal relationships that could have appeared to influence the work reported in this paper.

Acknowledgements

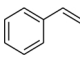
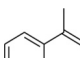
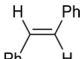
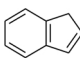
This work was supported by the Fundamental Research Funds for the Central Universities of China. This work was funded by the Researchers Supporting Project No. RSP-2020/1, King Saud University, Riyadh, Saudi Arabia.

Appendix A. Supplementary data

Supplementary material related to this article can be found, in the online version, at doi:<https://doi.org/10.1016/j.mcat.2020.111146>.

Table 6

Enantioselective epoxidation of unfunctionalized alkenes catalyzed by SBA-15-supported (tartrate-salen)Mn(III) polymer complexes under PhIO as terminal oxidant.

Entry ^a	Alkene	Catalyst ^b	Conversion ^c (%)	E.e. ^c (%)	TOF ^f
1		SBA-15	– ^d	–	–
2		Mn1@S	99 (95, 95, 96, 100)	78 (81, 88, 85, 76)/(R)	5.5
3		Mn1@aS	96	51 (S)	5.3
4		Mn2@S	96	78 (S)	5.3
5		Mn2@aS	91	47 (S)	5.0
6		Mn3@S	90	29 (S)	5.0
7		Mn3@aS	65	30 (S)	3.6
8		Mn4@S	90	42 (S)	5.0
9		Mn4@aS	79	2 (S)	4.3
10		Mn1@S	97 (97, 91, 85, 66)	94 (99, 95, 90, 89)/(R)	5.3
11		Mn1@aS	94 (97, 95, 89, 44)	92 (93, 95, 96, 92)/(R)	5.2
12		Mn2@S	99	51 (R)	5.5
13		Mn2@aS	90	43 (R)	5.0
14		Mn3@S	84	67 (R)	4.6
15		Mn3@aS	62	75 (R)	3.4
16		Mn4@S	34	43 (R)	1.8
17		Mn4@aS	32	22 (R)	3.4
18		Mn1@S	40	15 (R,R)	2.2
19		Mn1@aS	39	15 (R,R)	2.1
20		Mn2@S	28	0.2 (R,R)	1.5
21		Mn2@aS	29	1.8 (S,S)	1.6
22		Mn3@S	37	4 (S,S)	2.0
23		Mn3@aS	11	0.4 (R,R)	0.6
24		Mn4@S	26	12 (S,S)	1.4
25		Mn4@aS	1	0.1 (S,S)	0.05
26		Mn1@S	75	54 (1S,2R)	4.1
27		Mn1@aS	89	29 (1S,2R)	4.9
28		Mn2@S	77	45 (1S,2R)	4.2
29		Mn2@aS	69	81 (1S,2R)	3.8
30		Mn3@S	43	86 (1R,2S)	2.3
31		Mn3@aS	33	80 (1R,2S)	1.8
32		Mn4@S	88	24 (1R,2S)	4.8
33		Mn4@aS	78 (89, 90, 89, 100)	99 (99, 95, 76, 56)/(1R,2S)	4.3

^a Reaction conditions: alkene (1 mmol), NH₄OAc (co-catalyst, 0.12 mmol), PhIO (1 mmol), CH₂Cl₂ (5 mL), T (273 K), time (6 h).

^b SBA-15, 100 mg; catalyst loading was 3 mol% (Mn criteria).

^c Same as shown in Table 4, and data in parentheses represented consecutively recycled results.

^d No epoxides were found on HPLC.

^e Same as shown in Table 5 (Sect. A7, Supplementary data).

^f Turnover frequency of cycle fresh, mol_{product}/mol_{Mn}⁻¹(6 h)⁻¹, h⁻¹ as unit.

References

- [1] H. Cho, S. Katoh, S. Sayama, K. Murakami, H. Nakanishi, Y. Kajimoto, H. Ueno, H. Kawasaki, K. Aisaka, I. Uchida, Synthesis and selective coronary vasodilatory activity of 3,4-dihydro-2,2-bis(methoxymethyl)-2H-1-benzopyran-3-ol derivatives: Novel potassium channel openers, *J. Med. Chem.* 39 (1996) 3797–3805.
- [2] J.M. Wurst, G. Liu, D.S. Tan, Hydrogen-bonding catalysis and inhibition by simple solvents in the stereoselective kinetic epoxide-opening spirocyclization of glycol epoxides to form spiroketals, *J. Am. Chem. Soc.* 133 (2011) 7916–7925.
- [3] Y. Shi, Organocatalytic asymmetric epoxidation of olefins by chiral ketones, *Acc. Chem. Res.* 37 (2004) 488–496.
- [4] E.N. Jacobsen, Asymmetric catalysis of epoxide ring-opening reactions, *Acc. Chem. Res.* 33 (2000) 421–431.
- [5] J. Zhang, S. Wu, J. Wu, Z. Li, Enantioselective cascade biocatalysis via epoxide hydrolysis and alcohol oxidation: one-pot synthesis of (R)- α -hydroxy ketones from meso- or racemic epoxides, *ACS Catal.* 5 (2015) 51–58.
- [6] T. Katsuki, K.B. Sharpless, The first practical method for asymmetric epoxidation, *J. Am. Chem. Soc.* 102 (1980) 5974–5976.
- [7] E.N. Jacobsen, W. Zhang, M.L. Güler, Electronic tuning of asymmetric catalysts, *J. Am. Chem. Soc.* 113 (1991) 6703–6704.
- [8] R. Irie, K. Noda, Y. Ito, T. Katsuki, Enantioselective epoxidation of unfunctionalized olefins using chiral (salen)manganese(III) complexes, *Tetrahedron Lett.* 32 (1991) 1055–1058.
- [9] E.M. McGarrigle, D.G. Gilheany, Chromium- and manganese-salen promoted epoxidation of Alkenes, *Chem. Rev.* 105 (2005) 1563–1602.
- [10] S. Shaw, J.D. White, Asymmetric catalysis using chiral salen-metal complexes: recent advances, *Chem. Rev.* 105 (2005) 1603–1662.
- [11] R.I. Kureshy, T. Roy, N.H. Khan, S.H.R. Abdi, A. Sadhukhan, H.C. Bajaj, Reusable chiral macrocyclic Mn(III) salen complexes for enantioselective epoxidation of nonfunctionalized alkenes, *J. Catal.* 286 (2012) 41–50.
- [12] X. Yao, H. Chen, W. Lü, G. Pan, X. Hu, Z. Zheng, Enantioselective epoxidation of olefins catalyzed by two novel chiral poly-salen-Mn(III) complexes, *Tetrahedron Lett.* 41 (2000) 10267–10271.
- [13] T.S. Reger, K.D. Janda, Polymer-supported (salen)Mn catalysts for asymmetric epoxidation: a comparison between soluble and insoluble matrices, *J. Am. Chem. Soc.* 122 (2000) 6929–6934.
- [14] L. Lou, K. Yu, F. Ding, X. Peng, M. Dong, C. Zhang, S. Liu, Covalently anchored chiral Mn(III) salen-containing ionic species on mesoporous materials as effective catalysts for asymmetric epoxidation of unfunctionalized olefins, *J. Catal.* 249 (2007) 102–110.
- [15] R. Luo, R. Tan, Z. Peng, W. Zheng, Y. Kong, D. Yin, Stable chiral salen Mn(III) complexes with built-in phase-transfer capability for the asymmetric epoxidation of unfunctionalized olefins using NaOCl as an oxidant, *J. Catal.* 287 (2012) 170–177.
- [16] C.E. Song, S. Lee, Supported chiral catalysts on inorganic materials, *Chem. Rev.* 102 (2002) 3495–3524.
- [17] Q. Wang, D. O'Hare, Recent advances in the synthesis and application of layered double hydroxide (LDH) nanosheets, *Chem. Rev.* 112 (2012) 4124–4155.
- [18] R. Ryoo, C.H. Ko, Block-copolymer-templated ordered mesoporous silica: array of uniform mesopores or mesopore–micropore network? *J. Phys. Chem. B* 104 (2000) 11465–11471.
- [19] J. Scholz, A. Walter, T. Ressler, Influence of MgO-modified SBA-15 on the structure and catalytic activity of supported vanadium oxide catalysts, *J. Catal.* 309 (2014) 105–114.
- [20] M. Choi, W. Heo, F. Kleitz, R. Ryoo, Facile synthesis of high quality mesoporous SBA-15 with enhanced control of the porous network connectivity and wall thickness, *Chem. Commun.* (2003) 1340–1341.
- [21] F. Teixeira, R.A. Mosquera, A. Melo, C. Freire, M. Natália, D.S. Cordeiro, Effects of axial coordination on immobilized Mn(salen) catalysts, *J. Phys. Chem. A* 118 (2014) 10788–10796.
- [22] K.K. Bania, G.V. Karunakar, K. Goutham, R.C. Deka, Enantioselective Henry reaction catalyzed by “Ship in a Bottle” complexes, *Inorg. Chem.* 52 (2013) 8017–8029.
- [23] L. Canali, E. Cowan, H. Deleuze, C.L. Gibson, D.C. Sherrington, Remarkable matrix effect in polymer-supported Jacobsen's alkene epoxidation catalysts, *J. Chem. Soc., Perkin Trans. 1* (2000) 2055–2066.
- [24] C. Hess, J.D. Hoefelmeyer, T.D. Tilley, Spectroscopic characterization of highly dispersed vanadia supported on SBA-15, *J. Phys. Chem. B* 108 (2004) 9703–9709.
- [25] K. Yu, Z. Gu, R. Ji, L. Lou, F. Ding, C. Zhang, S. Liu, Effect of pore size on the performance of mesoporous material supported chiral Mn(III) salen complex for the epoxidation of unfunctionalized olefins, *J. Catal.* 252 (2007) 312–320.
- [26] P. Piaggio, C. Langham, P. McMorn, D. Bethell, P.C. Bulman-Page, F.E. Hancock, C. Sly, G.J. Hutchings, Catalytic asymmetric epoxidation of stilbene using a chiral salen complex immobilized in Mn-exchanged Al-MCM-41, *J. Chem. Soc., Perkin Trans. 2* (2000) 143–148.
- [27] D. Zhao, J. Feng, Q. Huo, N. Melosh, G.H. Fredrickson, B.F. Chmelka, G.D. Stucky, Triblock copolymer synthesis of mesoporous silica with periodic 50 to 300 angstrom pores, *Science* 279 (1998) 548–552.
- [28] I.D. Kostas, F.J. Andreadaki, D. Kovala-Demertzi, C. Prentzas, M.A. Demertzis, Suzuki–Miyaura cross-coupling reaction of aryl bromides and chlorides with phenylboronic acid under aerobic conditions catalyzed by palladium complexes with thiosemicarbazone ligands, *Tetrahedron Lett.* 46 (2005) 1967–1970.
- [29] P. Alreja, N. Kaur, Recent advances in 1,10-phenanthroline ligands for chemosensing of cations and anions, *RSC Adv.* 6 (2016) 23169–23217.
- [30] K.S.W. Sing, D.H. Everett, R.A.W. Haul, L. Moscou, R.A. Pierotti, J. Rouquerol, T. Siemieniowska, Reporting physisorption data for gas/solid systems with special reference to the determination of surface area and porosity, *Pure Appl. Chem.* 57 (1985) 603–619.
- [31] M.T. Le, T.T. Nguyen, P.T.M. Pham, E. Bruneel, I.V. Driessche, Activated MnO₂-Co₃O₄-CeO₂ catalysts for the treatment of CO at room temperature, *App. Catal. A: Gen.* 480 (2014) 34–41.
- [32] W. Zhang, J.L. Loebach, S.R. Wilson, E.N. Jacobsen, Enantioselective epoxidation of unfunctionalized olefins catalyzed by salen manganese complexes, *J. Am. Chem. Soc.* 112 (1990) 2801–2803.
- [33] K. Malek, C. Li, R.A. van Santen, New theoretical insights into epoxidation of alkenes by immobilized Mn-salen complexes in mesopores: effects of substrate, linker and confinement, *J. Mol. Catal. A Chem.* 271 (2007) 98–104.
- [34] C.E. Song, E.J. Roh, Practical method to recycle a chiral (salen)Mn epoxidation catalyst by using an ionic liquid, *Chem. Commun.* (2000) 837–838.
- [35] J. Zhao, Y. Zhang, F. Han, S. Zhao, Asymmetric epoxidation of unfunctionalized alkenes catalyzed by sugar moiety-modified chiral salen-Mn(III) complexes, *Carbohydr. Res.* 344 (2009) 61–66.
- [36] K. Malek, A.P.J. Jansen, C. Li, R.A. van Santen, Enantioselectivity of immobilized Mn-salen complexes: a computational study, *J. Catal.* 246 (2007) 127–135.